J. Fluid Mech. (1980), *vol.* 97, *part* 1, *pp.* 27–51
Printed in Great Britain

Internal separated flows at large Reynolds number

By ANAND KUMAR AND KIRIT S. YAJNIK
Aerodynamics Division, National Aeronautical Laboratory, Bangalore 560017, India

(Received 28 October 1977 and in revised form 1 June 1979)

Large-Reynolds-number analysis is given for separated flows that have the characteristic feature of being confined in the transverse direction. Two principal limits of the governing equation are obtained depending on whether the streamwise length scale is of order one or of the order of the Reynolds number. The corresponding two types of separated flows are discussed. A method of calculation is given for the second type of flow. It employs an expansion in the eigenfunctions of the Poiseuille flow development and the problem is reduced to solving nonlinear first-order ordinary differential equations that have a tendency to decouple rapidly. The method is tested by a detailed comparison of the results of the present calculation with finite-difference solutions of the Navier–Stokes equations for a channel with sudden expansion. Applicability to other configurations is illustrated by solving the problem of the flow in a channel with a base.

1. Introduction

A large-Reynolds-number solution of attached flow past a body can be obtained by using perturbation techniques. However when the flow separates from the body, it presents certain difficulties which are not yet well understood. In this paper we examine internal separated flows (figure 1) which are less complex than external separated flows. Although the interplay between the wake and the outer flow is absent in the present case, there are other features which are common with external separated flows, e.g. thick recirculating regions. The major simplifying feature is that the transverse length scale is of order one on account of the walls confining the flow.

Hung & Macagno (1966) have obtained a finite-difference solution of the Navier–Stokes equations for internal separated flow in a channel with a symmetric sudden expansion. Morihara (1972) has also solved this problem by using a finite-difference scheme. Flow in a gradually widening channel has been considered by Dorodnitsyn & Meller (1970). Numerical investigation of separated flow in a channel with a back-step, or with single or multiple obstructions, has been carried out by Nallasamy (1975). Other internal separated flows studied by various investigators include a channel with a constriction (Greenspan 1969; Friedman 1972; Cheng 1972), a channel with a back-step (Mueller & O'Leary 1970; Roache & Mueller 1970; Taylor & Ndefo 1970), a channel with a forward-step (Greenspan 1969), a channel with a base (Mueller & O'Leary 1970) and a channel wth a symmetric contraction (Morihara 1972). However these investigators have been concerned primarily with computational procedures.

We first consider large-Reynolds-number limits of the governing equation; attention is focused on limit equations. Two types of separated flows, suggested by the two

0022–1120/80/4386–8340 $02.00

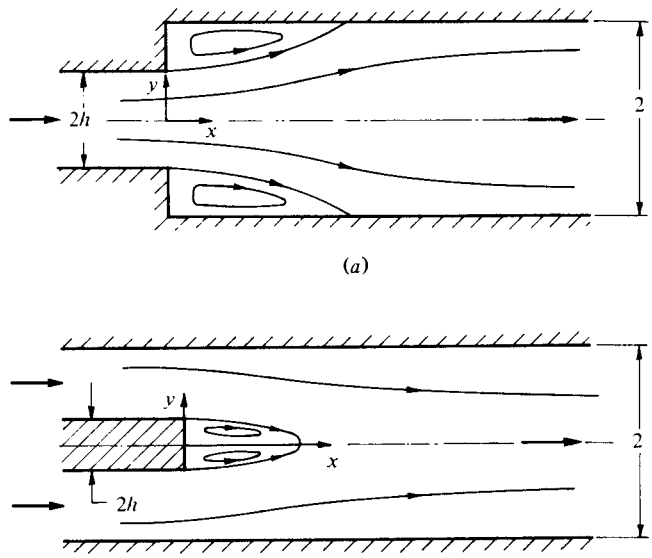

FIGURE 1. Internal separated flow problems. (*a*) A channel with a symmetric sudden expansion. (*b*) A channel with a base.

limit equations, are discussed. A method of calculation based on the appropriate limit equation is developed for the types of separated flow shown in figure 1. The method uses an expansion in the eigenfunctions of the Poiseuille-flow development. Calculations require the solution of a set of ordinary differential equations that get progressively decoupled in the downstream direction. Results have been obtained for configurations in which the channel has a symmetric expansion, a back-step or a base (Kumar 1976). A few of these results are discussed in this paper.

2. Limit equations

We consider steady, two-dimensional laminar motion of an incompressible Newtonian fluid. The governing equation in the non-dimensional form is

$$\psi_y \nabla^2 \psi_x - \psi_x \nabla^2 \psi_y = R^{-1} \nabla^4 \psi, \tag{1}$$

where ψ is the stream-function, R is the Reynolds number, and suffixes x and y denote partial derivatives.

Let the length scales in the x and y directions be L_x and L_y, and the scale of the streamwise velocity u be U. The transverse length scale L_y is of order one in the present set of problems. If we examine possible limits for the bulk of the flow region where $U \sim 1$ we find that there are two principal limits corresponding to $L_x \sim 1$ and $L_x \sim R$, if the flow velocity is bounded.† The limit equation for $L_x \sim 1$ is the Euler equation

$$\psi_y \nabla^2 \psi_x - \psi_x \nabla^2 \psi_y = 0. \tag{2}$$

† Various limit equations of (1) and their domains of validity are considered by Kumar (1976).

The limit equation for $L_x \sim R$ is

$$\psi_y \psi_{yyx} - \psi_x \psi_{yyy} = R^{-1} \psi_{yyyy}. \tag{3}$$

Limit equation (2) is elliptic in nature whereas (3) is a parabolic equation. We therefore expect that (2) applies to both the upstream and the downstream type of effects and (3) to the downstream type of effect only.

The applicability of the two principal limits can be illustrated by considering the spatial behaviour of disturbances of Poiseuille flow. A small perturbation analysis based on the Navier–Stokes equations is given by Wilson (1969). Perturbation which is of the form $\phi(y) \exp(-\lambda x)$ leads to an eigenvalue problem which has two sequences of eigenvalues for large R. The first sequence contains eigenvalues of order one, and the other, of order $1/R$. An eigenvalue of order one implies that the perturbation decays over a distance of order one. These eigenvalues are positive as well as negative, and therefore the associated perturbations are felt downstream and upstream. The eigenvalues of the second sequence are such that the perturbation decays over a distance of order R in the downstream direction. The disturbances are thus felt upstream up to a distance of order one and downstream up to a distance of order R. Both the limiting eigenvalue problems considered by Wilson can be obtained from (2) and (3). The order of the eigenvalues and their signs are thus what may be expected from the nature of (2) and (3).

3. Two classes of internal separated flow

The two limit equations suggest that there are two classes of flows where either (2) or (3) characterizes the large-Reynolds-number behaviour. It is understood that there might be subregions where the solution of (2) or (3) is singular and therefore supplementary limits are required.

Two simple configurations illustrating these situations are given in figure 2. In the case of sudden contraction, the flow separates upstream of the configuration responsible for it. We then expect such flows to be governed by (2). These flows are essentially inviscid. In such cases the arguments of Prandtl (1904) and Batchelor (1956) would be applicable to the recirculating region.†

Flow separation occurs in the case of sudden expansion on the downstream side. While it is compatible with both (2) and (3), the latter is expected to govern the bulk of the flow, as its associated streamwise length scale is larger. The streamwise length scale for such flow will therefore be of order R. That is, a typical length scale, such as the length of the recirculating region, behaves as R; this conclusion can also be reached by the following argument. When $L_x \sim 1$ and $L_y \sim 1$, viscous terms are of higher order. In this 'near' limit, the flow is governed by the Euler equation whose solution allows discontinuous surfaces. One such surface is along the separating streamline. A vorticity layer is required for the vorticity to diffuse in the recirculating region. The thickness of this layer is of order $(x/R)^{\frac{1}{2}}$, and therefore for any fixed x, it shrinks to zero in the limit.

† Applicability of (2) requires that L_x is of order one for such flows. On the other hand, Smith (1977) has given an analysis which applies only to asymmetric flows, and which requires the upstream length scale to increase as $R^{\frac{1}{7}}$. However, we are of the view that it is unlikely that the length of the upstream recirculating region increases indefinitely with Reynolds number.

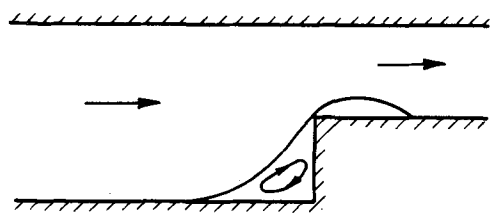

(a)

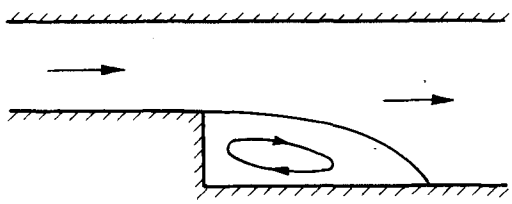

(b)

FIGURE 2. Schematic diagrams of two types of internal separated flow: (a) first type; (b) second type.

When $x \sim R$, the vorticity layer thickness is of the order of the transverse length scale of the channel itself. The 'near' limit is therefore inapplicable when $x \sim R$. A 'far' limit given by $L_x \sim R$ is required which leads to (3). While this argument brings out the nature of the separated flow downstream of a sudden expansion, a similar argument does not reveal the nature of the separated flow upstream of a sudden contraction.

We now examine earlier numerical calculations to test the above conclusions regarding the two different types of separated flows. We look for the streamwise length scale in these calculations.

Hung & Macagno (1966) have obtained the finite-difference solution of the Navier–Stokes equations for flow in a channel with a symmetric sudden expansion. Velocity profile upstream of the expansion is taken to be parabolic. Figure 3 shows the behaviour of the distance of the point of reattachment and the distance of the centre of the eddy measured from the expansion. A linear trend is clearly seen for large R. Results obtained by Morihara (1972) for the above problem also show a linear trend (figure 3).

Mueller & O'Leary (1970) have done numerical calculations as well as experiments on a channel with a back-step and with a base. Their results show that for large Reynolds number the reattachment length and the distance of the centre of eddy from the step vary linearly with the Reynolds number. A similar trend is also shown by the calculation for flow past a square proturberance in a Couette flow (Kitchens 1974).

Cheng (1972) has given finite element solutions of the Navier–Stokes equations for values of R up to 100 for flow in a channel with a smooth constriction. Upstream separation does not occur for the range of R considered. However the effect of the constriction can be inferred from the plot of wall vorticity for different values of R.

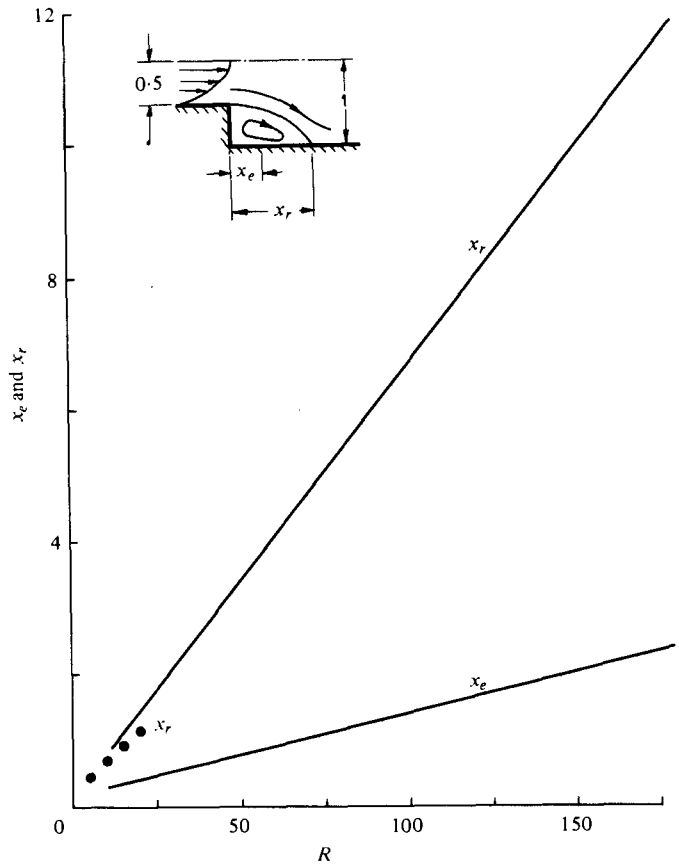

FIGURE 3. Variation of streamwise length scale with R. ——, Hung & Macagno (1966); ●, Morihara (1972).

While the upstream influence is confined to a short distance, the extent of downstream influence increases with R.†

Flow in the presence of a two-dimensional grid is considered by Kovasznay (1948). As $L_y \sim 1$, the present arguments about the limiting behaviour of the flow upstream and downstream of the grid would be applicable. A study of the solutions of the Oseen equations also shows qualitative agreement, namely that the flow upstream of the grid is affected up to a length of order one while that downstream up to a length of order R. These solutions include the flows given by Kovasznay.

Thus the earlier calculations based on the Navier–Stokes equations support our view of two qualitatively different types of separated flows. They differ in their respective streamwise length scales and the limit equations governing the bulk of the flow. The recirculating region which occurs ahead of a contraction is essentially inviscid. However, the dynamics of the recirculating region appearing downstream of an expansion is such that viscous forces, being of the same order as inertia forces, are retained. Internal separated flows of this class are further examined in the following sections.

† Similar conclusions can also be drawn for the axisymmetric case and they are supported by numerical calculations based on complete equations (see appendix A).

4. Formulation of the problem

Consider the flow in a channel with a sudden expansion which belongs to the second type of internal separated flow as a prototype for our discussion here. The flow downstream of the expansion is divided into two subregions corresponding to $L_x \sim 1$ and $L_x \sim R$. The limit equation for the 'far' region ($L_x \sim R$) is (3). As a result of the limiting process, three derivatives in x are lost. Therefore (3) can satisfy only one condition in x, which is obtained by matching with the solution for the 'near' region ($L_x \sim 1$).

The 'near' region solution is in general difficult to construct. In the case of a parallel incoming flow, a possible free-streamline solution of the Euler equation consists of the incoming flow and a zero velocity behind the step. That is, the incoming flow goes undisturbed through the 'near' region to the lowest order. Although there are an infinite number of solutions of the Euler equation, the above solution would seem a likely candidate that matches with the far downstream flow.

The equation governing the 'far' region can be written as

$$\psi_y \psi_{yyx} - \psi_x \psi_{yyy} = \psi_{yyyy}, \tag{4}$$

where the x co-ordinate has been scaled by R. Unless otherwise stated, x would henceforth imply the contracted streamwise co-ordinate. R is based on the average velocity and the half-width of the channel downstream of the expansion.

Since the 'near' region shrinks to $x = 0$ in the newly scaled co-ordinate, (4) can be regarded as the field equation for $x > 0$. The initial condition required for the integration of (4) is obtained from matching

$$\psi(x \to 0, y) = \psi_0(y). \tag{5}$$

This condition is equivalent to prescribing u_0, the streamwise velocity at the inlet section. The incoming flow is taken to be a parallel flow in the examples considered in this paper. Then u_0 is the incoming flow velocity distribution. The conditions at the walls require

$$\psi = \pm 1, \quad \psi_y = 0 \quad \text{at} \quad y = \pm 1. \tag{6}$$

The problem then is to obtain the solution of (4) satisfying conditions (5) and (6). Equation (4) can be integrated once with respect to y. The constant of integration is the pressure gradient. However, it is preferable to work with (4) than with its integral.

The limit equation (4) is similar to the boundary-layer equations. However, it should be noted that the viscous region has a thickness of order one whereas the thickness of the classical boundary layer is of order $R^{-\frac{1}{2}}$. Also, instead of pressure being impressed by the external flow, it has to be obtained as a part of the calculation here. This is possible as there are four boundary conditions in y. The confinement of the flow can thus be said to generate its own pressure field.

In the presence of reverse flow, (4) is said to be of the mixed parabolic type. The theory of such equations has not yet been sufficiently developed to indicate the boundary conditions which would lead to a solution. The present problem arises from a limit process on an elliptic equation which presumably has a solution whose above limit exists. It is then reasonable to assume that the problem posed here has a solution.

5. Method of solution

Numerical integration of parabolic equation is usually performed by a marching type, finite-difference scheme. However, Klemp & Acrivos (1972), Klineberg & Steger (1974) and Carter (1975) have used iterative finite-difference schemes to integrate the boundary-layer equations. In these schemes the x derivatives are differenced depending on the direction of the flow.† A marching type finite-difference scheme is used by Catherall & Mangler (1966) to solve for boundary layer with separation and reattachment.

We use an integral relations method of solution. The method requires a set of functions for expansion and a set of weighting functions. The functions are chosen for their properties. While series representations with a large number of terms, as many as fifty, have been used, a judicious choice of expansion and weighting functions can considerably reduce the computation. The flow at large downstream distances is a small perturbation of the Poiseuille flow which leads to a linear eigenvalue problem. Its eigenfunctions are used as the expansion set whose coefficients depend on the streamwise co-ordinate. The eigenfunctions of the adjoint problem are the weighting functions. The resulting set of coupled ordinary differential equations tend to get progressively decoupled with streamwise distance. These functions are in this sense natural to the present problem.

5.1. *The eigenvalue problem*

We first review the eigenvalue problem. The channel flow develops into Poiseuille flow $\psi_P = \frac{1}{2}(3y - y^3)$. Let ψ be expressed as a sum of ψ_P and a perturbation ψ_1. The equation governing ψ_1 is then obtained from (4) as

$$\psi_{1yyyy} - \psi'_P \psi_{1yyx} + \psi'''_P \psi_{1x} = \psi_{1y} \psi_{1yyx} - \psi_{1x} \psi_{1yyy}, \tag{7}$$

where primes denote differentiation. When ψ_1 is small, the quadratic terms in ψ_1 may be neglected and we get the linearized equation,

$$\psi_{1yyyy} - \tfrac{3}{2}(1 - y^2)\psi_{1yyx} - 3\psi_{1x} = 0. \tag{8}$$

The above equation has solutions of the form

$$\psi_1 = \phi(y)\, e^{-\lambda x}, \tag{9}$$

where ϕ is an eigenfunction and λ the corresponding eigenvalue of the eigenvalue problem,

$$\phi^{iv} + \lambda[\tfrac{3}{2}(1 - y^2)\phi'' + 3\phi] = 0,$$

$$\phi = \phi' = 0 \quad \text{at} \quad y = \pm 1. \tag{10}$$

† Such schemes are sometimes regarded as devices to incorporate upstream influence in the reverse flow region. However, the associated differencing error is equivalent to introducing certain higher-order derivatives into the equation (Kumar 1978). It would therefore seem that the numerical scheme provides a mechanism for upstream influence. As the coefficients of the higher-order derivatives are proportional to certain positive powers of the step size, this mechanism of upstream influence tends to vanish as the step size is reduced. Detailed numerical experiments (Kumar 1978) support this view.

	λ_m	
m	Odd	Even
1	14·45	
2		18·81
3	48·87	
4		57·52
5	104·43	
6		117·30
7	181·25	
8		198·26
9	279·38	
10		300·50

TABLE 1. Eigenvalues of equation (10).

Clearly, the solutions of (10) can be separated into even and odd solutions. An eigenfunction is called even or odd depending on the symmetry or the antisymmetry of ϕ' which is related to the streamwise velocity component.

Equation (10) can be integrated once and the constant of integration, which is related to the pressure gradient, turns out to be zero for odd eigenfunctions. Consequently, the pressure field is uniform in the case of a small antisymmetric streamwise velocity perturbation.

Wilson (1969) has obtained (10) as the equation governing the leading term in a large R expansion and has shown that the odd eigenvalues are real. A similar result is not available for even eigenvalues. However, if the eigenvalues of (10) are real, they can be shown to be positive by multiplying (10) by ϕ and integrating by parts. Based on the numerical evidence we have taken the eigenvalues to be real.

Table 1 contains the first ten eigenvalues.† They are numbered in increasing order and are alternately odd and even. The lowest eigenvalue is odd, and hence the velocity perturbation which persists the longest is antisymmetric. The first five eigenvalues are in agreement with those given by Wilson (1969).

Analysis of equation (10) for large λ, which is somewhat similar to that for the Orr–Sommerfeld equation, gives (Kumar 1977)

$$\lambda_m \sim \tfrac{32}{3}(n+\tfrac{1}{12})^2 \quad m = 2n+1 \quad \text{odd}, \tag{11a}$$

$$\lambda_m \sim \tfrac{32}{3}(n+\tfrac{1}{4})^2 \quad m = 2n+2 \quad \text{even}. \tag{11b}$$

The adjoint eigenvalue problem is

$$\theta^{\mathrm{iv}} + \lambda[\tfrac{3}{2}(1-y^2)\theta'' - 6y\theta'] = 0,$$

$$\theta = \theta' = 0 \quad \text{at} \quad y = \pm 1. \tag{12}$$

If ϕ_p and θ_q are eigenfunctions of (10) and (12) respectively and the corresponding eigenvalues are λ_p and λ_q, it can be shown that

$$\int_{-1}^{1} \phi_p'' \theta_q'' \, dy = 0 \quad p \neq q. \tag{13}$$

† These values are obtained by using the Runge–Kutta–Gill method of integration with a step size of 0·02 and double precision. Further ten eigenvalues are given by Kumar (1977).

We assume that the functions satisfying certain conditions can be expanded in a convergent series of the eigenfunctions ϕ_m. Let f be expanded as

$$f = \sum_{m=1}^{\infty} b_m \phi_m. \tag{14}$$

The coefficient b_m is then obtained by multiplying (14) by θ_m^{iv} and integrating,

$$b_m = G_m^{-1} \int_{-1}^{1} f \theta_m^{\mathrm{iv}} \, dy, \tag{15}$$

where

$$G_m = \int_{-1}^{1} \phi_m'' \theta_m'' \, dy. \tag{16}$$

If ψ_1 is sufficiently small so that the linear equation (8) can be used for $x \geqslant x_0$, the solution is given by

$$\psi_1(x, y) = \sum_{m=1}^{\infty} A_m e^{-\lambda_m (x - x_0)} \phi_m(y), \tag{17a}$$

where

$$A_m = G_m^{-1} \int_{-1}^{1} \psi_1(x_0, y) \, \theta_m^{\mathrm{iv}} \, dy. \tag{17b}$$

5.2. *The eigenfunction expansion method*

The method of calculation† is based on taking the stream function in the form

$$\begin{aligned} \psi(x, y) &= \psi_P(y) + \psi_1(x, y), \\ &= \psi_P(y) + \sum_m a_m(x) \, \phi_m(y). \end{aligned} \tag{18}$$

We truncate the series after, say, N terms. Only even eigenfunctions are considered in a symmetric solution and the index m runs over the first N even eigenfunctions. The following N ordinary differential equations are obtained by substituting (18) in (4), multiplying by θ_m and integrating.

$$a_m' + \lambda_m a_m = \sum_p \sum_q C_{mpq} a_p' a_q, \tag{19}‡$$

where

$$C_{mpq} = \lambda_m G_m^{-1} \int_{-1}^{1} \theta_m' (\phi_p \phi_q'' - \phi_p' \phi_q') \, dy. \tag{20}$$

The first term on the left-hand side in (19) arises from the linearized part of the inertia term whereas the transverse viscous diffusion is represented by the second term. The nonlinear interaction of the modes is given by the terms on the right-hand side.

† This method is designed for the homogeneous boundary conditions (6). There are many variations of the problems in which the boundary conditions have a different form, e.g. curved walls, non-zero tangential or normal velocity. The method described here is not expected to apply to these situations without some modification.

‡ If another set of functions, f_n, e.g. polynomials, are used in the place of the eigenfunctions, one obtains a set of differential equations similar to (19) but with different coefficients, that is

$$\sum_n (D_{mn} a_n' + \Delta_{mn} a_n) = \sum_p \sum_q C_{mpq} a_p' a_q,$$

where D_{mn}, Δ_{mn} and C_{mpq} are integrals depending on f_n. Clearly, (19) is a particular case of the above. However, the use of ϕ_m has certain advantages as we shall see.

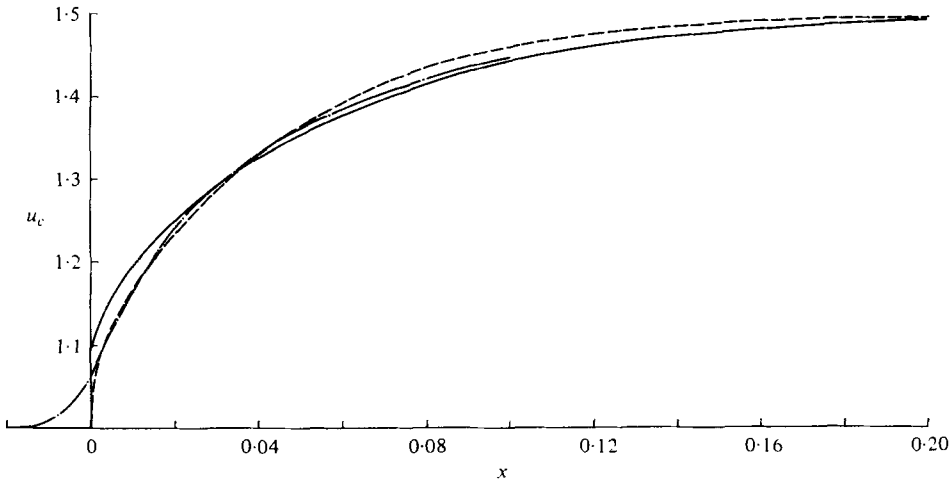

FIGURE 4. Centre-line velocity distribution for the entry flow in a channel. ——, Kumar & Yajnik (1976); – – –, Morihara (1972), $R = 1000$; —·—·—, Wang & Longwell (1964), $R = 75$.

The initial condition for (19) is obtained by evaluating (18) at $x = 0$, multiplying by θ_m^{iv} and integrating,

$$a_{m0} = a_m(0) = G_m^{-1} \int_{-1}^{1} \psi_1(0, y)\, \theta_m^{\mathrm{iv}}\, dy. \tag{21}$$

If $\psi_1(0, y)$ is piecewise twice differentiable, the above relation can be simplified to

$$a_{m0} = G_m^{-1} \int_{-1}^{1} \psi_0'' \theta_m''\, dy. \tag{22}$$

The problem is thus reduced to solving a set of N first-order ordinary differential equations (19), subject to the initial condition (21). These equations are coupled, quasi-linear and autonomous.†

6. Illustrative calculations

The entry flow in a channel is first considered with a view to test the method of calculation. Morihara (1972), Wang & Longwell (1964) and Gillis & Brandt (1964) have made finite-difference calculations of the Navier–Stokes equations for this problem. Centre-line velocity, pressure gradient, and skin friction obtained by the present method are compared with the earlier results (Kumar & Yajnik 1976). Figure 4 compares the present centre-line velocity distribution with those given by Morihara (1972) and Wang & Longwell (1964). The calculation of Morihara is for a uniform

† Equation (19) can be written in the form

$$\sum_p (\delta_{mp} - \sum_q C_{mpq} a_q)\, a_p' = -\lambda_m a_m,$$

where δ_{mp} is the Kronecker delta. These equations are linear algebraic equations for a_p' for given a_m at a certain x and they can be solved provided the determinant D of the coefficient matrix is not zero. If D becomes zero at any x during the calculation of a solution, the calculation cannot in general be executed. This is further discussed in appendix B.

inlet flow, while the flow is taken by Wang & Longwell to be uniform far upstream of the inlet. The comparisons are found to be good slightly away from the inlet. Also, the calculated velocity profiles show qualitative features like a boundary layer with a uniform central core as assumed by Schlichting (1934), over a certain intermediate range of x (Kumar & Yajnik 1976). It is also found that the addition of higher modes improves the agreement near the inlet.

Several problems involving recirculating regions have been solved by the present method whose results are described elsewhere (Kumar 1976). Here we restrict ourselves to a discussion of two separated flow calculations.† The first problem, which also serves as a test case, deals with flow in a channel with a sudden expansion. Flow behind a base in a channel is considered next.

6.1. *Channel with a symmetric sudden expansion*

The entry flow u_0 is taken to be parabolic

$$u_0 = \frac{3}{2h}[1-(y/h)^2] \quad 0 \leqslant y \leqslant h,$$

$$= 0 \quad h \leqslant y \leqslant 1, \tag{23}$$

where h is the half-width of the channel upstream of the expansion. The ratio of expansion defined as the ratio of downstream channel width to that upstream of the expansion, is given by $1/h$. The initial condition a_{m0} obtained from (23) by using (21) or (22) is

$$a_{m0} = -6[h\theta'_m(h) - \theta_m(h)]/(G_m h^3), \tag{24}$$

where G_m is given by (16). The calculations with $N = 2$, 3 and 5 are sufficient to bring out the main features of the solution as well as the method.

The assumed parabolic entry profile (23) is shown in figure 5 with its approximations. We find that the approximation of the given velocity profile improves with increasing N. Table 2 compares the centre-line velocity u_{c0} and the associated momentum flux M_0 with the actual value. Clearly, the approximation tends to improve with the inclusion of higher modes.

Streamlines based on the calculation with $N = 3$ for $h = 0{\cdot}5$ are compared in figure 6 with those given by Hung & Macagno (1966). It is seen that the present streamline pattern is in good qualitative agreement with that obtained by Hung & Macagno. The flow characteristics are compared in table 3. x_r and x_e are streamwise co-ordinates of the point of reattachment and the centre of the eddy respectively. Total recirculation in one eddy is given by $(\psi_e - 1)$, and $\omega_{+\min}$ denotes the minimum vorticity at the upper wall of the channel which is proportional to minimum wall shear. The quantitative predictions are also seen to be in good agreement.

† The integration procedure adopted for (19) proceeds in the phase space. At each step of integration on a_m for which $|a'_m|$ is the largest, is chosen to be the independent variable. A predictor–corrector method with variable step size is used. An outline of the computer programme is given in Kumar (1976). Also a step size along y of 0·05 is used to obtain the eigenfunctions required to evaluate C_{mpq}. A finer step size would be needed for higher eigenfunctions as they oscillate more rapidly.

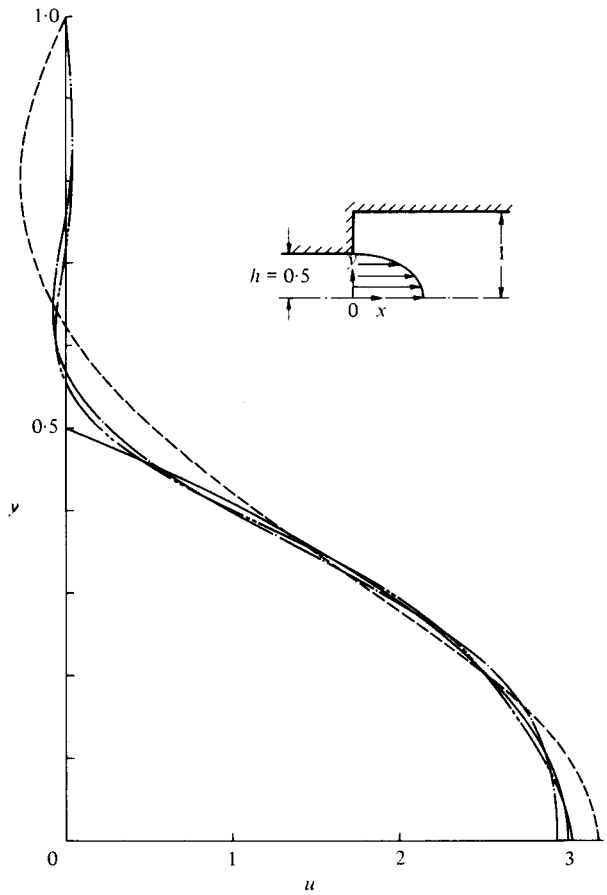

FIGURE 5. Representation of the entry condition, $h = 0{\cdot}5$. ——, given. Represented: ——, $N = 2$; —·—·—, $N = 3$; —··—··—, $N = 5$.

N	2	3	5	Given
u_{c0}	3·188	2·937	3·025	3·0
M_0	2·555	2·385	2·384	2·4

TABLE 2. Representation of the entry profile for symmetric sudden expansion ($h = 0{\cdot}5$).

	x_r	x_s	$(\psi_s - 1)$	$\omega_{+\min}$
Hung & Macagno (1966)	0·066	0·013	0·052	−2·82
Present calculation, $N = 3$	0·064	0·014	0·045	−2·19

TABLE 3. Comparison of present calculation ($h = 0{\cdot}5$) with that of Hung & Macagno (1966).

The centre-line velocity u_c is shown in figure 7. Calculations with $N = 3$ and 5 give almost the same u_c except very close to the expansion. Although a very small number of terms are used, the results indicate a convergent trend. Velocity profiles at various streamwise locations are shown in figure 8.

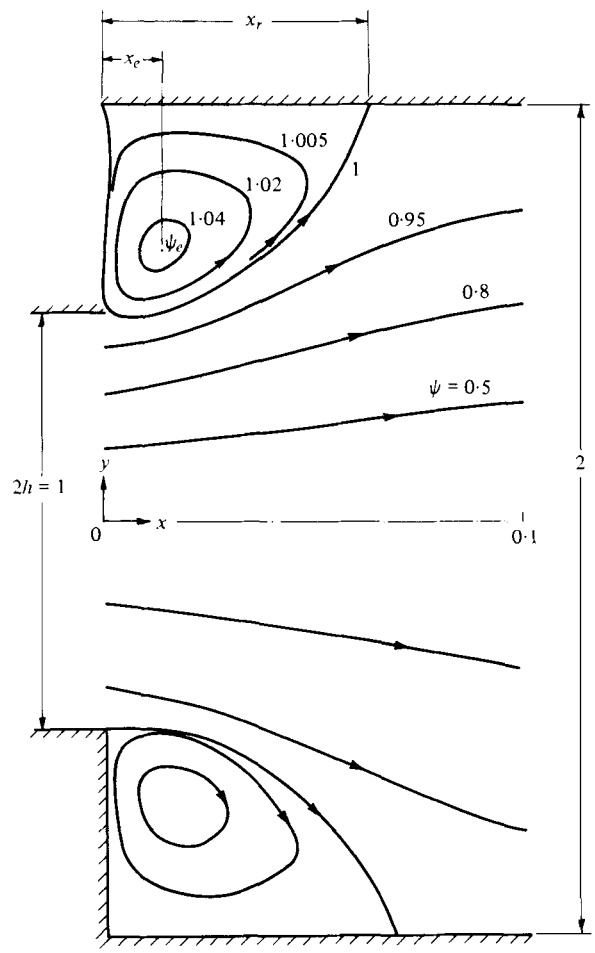

FIGURE 6. Streamlines obtained by the present method (top half of figure) and given by Hung & Macagno (1966) (bottom half of figure), $h = 0{\cdot}5$, $N = 3$. $R = 46{\cdot}6$ for Hung & Macagno results.

Pressure gradient and wall-vorticity are shown in figures 9 and 10 respectively. The effects of increase in N are most felt close to the expansion and they are generally larger than those on the centre-line velocity. This is due to the dependence of dp/dx and ω on the third and second derivatives of the eigenfunctions respectively. But, as $a_m(x)$ for the higher modes decay more rapidly, the calculations show a convergent trend away from the inlet. We expect that the results close to the inlet can be improved by increasing N. However, if the interest is mainly in flow features away from the inlet, a few terms are adequate to give good results.

Pressure is obtained by integrating dp/dx (figure 11). The curve at large x is translated by the integrated effect of changes in dp/dx near the inlet as N is increased. It is to be noted that the point of reattachment, also shown in figure 11, precedes a region where pressure levels off, which is a common feature of separated flows.

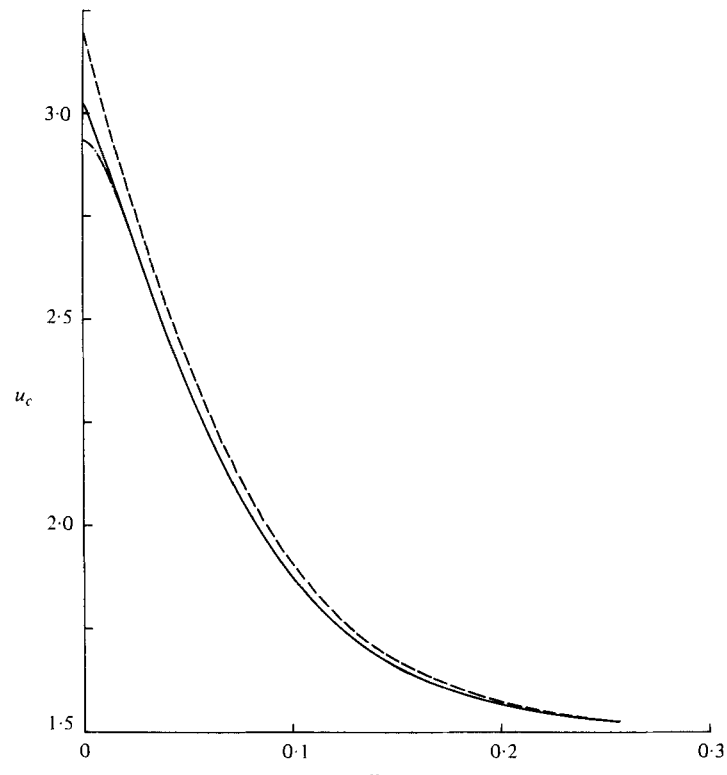

FIGURE 7. Centre-line velocity distribution, $h = 0{\cdot}5$. – – –, $N = 2$; — · — · —, $N = 3$; ——, $N = 5$.

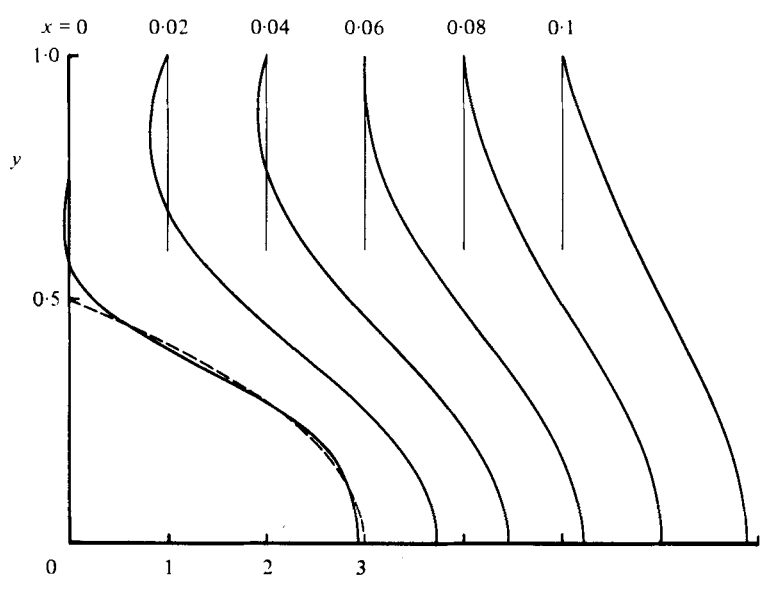

FIGURE 8. Streamwise velocity profile at various x, $h = 0{\cdot}5$. $N = 3$.
——, calculated; – – –, given at $x = 0$.

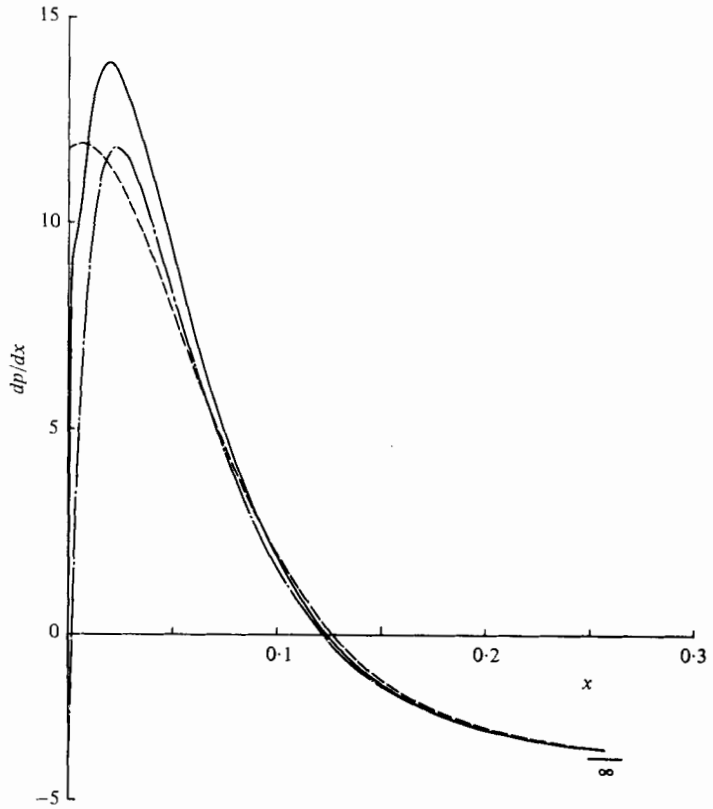

FIGURE 9. Distribution of pressure gradient, $h = 0{\cdot}5$. – – –, $N = 2$; — · — · —, $N = 3$; ——, $N = 5$.

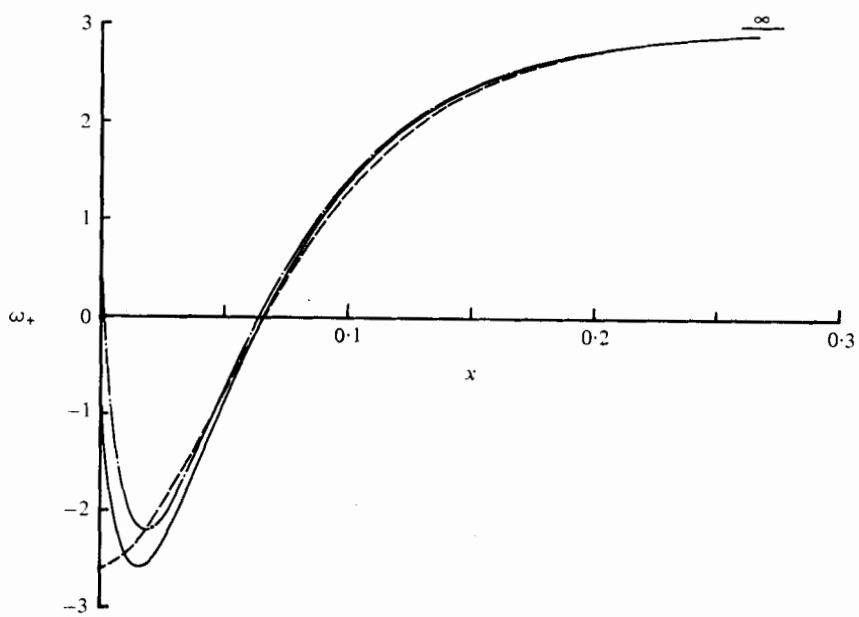

FIGURE 10. Distribution of vorticity at the upper wall, $h = 0{\cdot}5$. The lines are as in figure 9.

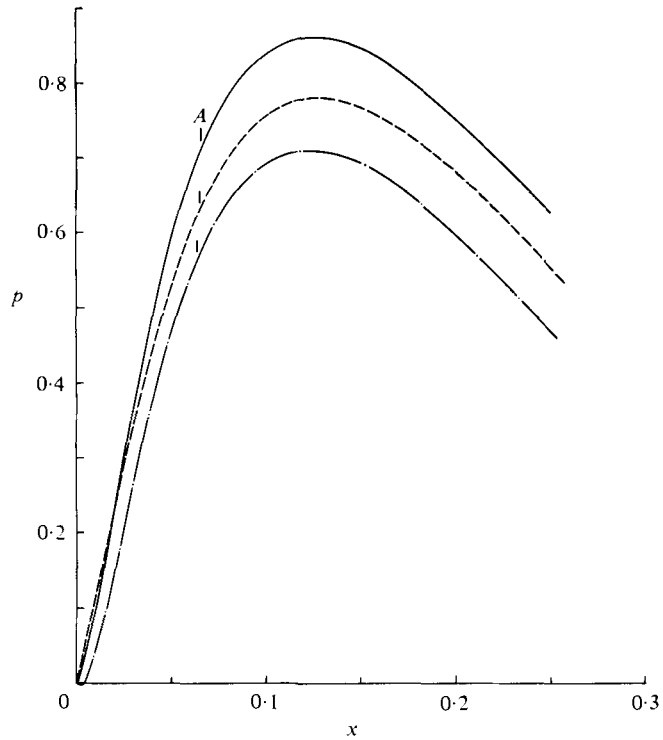

FIGURE 11. Pressure distribution, $h = 0{\cdot}5$. The lines are as in figure 9. A denotes point of reattachment.

N	x_r	x_d	P_r
2	0·0659	0·2839	1·320
3	0·0638	0·2779	1·234
5	0·0656	0·2775	1·390

TABLE 4. Comparison of calculations with different N ($h = 0{\cdot}5$).

Table 4 compares x_r, the development length x_d, and the pressure recovery coefficient P_r for different N.† It is seen that the prediction of x_r and x_d is not sensitive to N. The effect of N on P_r is larger which is to be expected for the reason mentioned earlier.

Figure 12 shows the effect of the expansion ratio $1/h$ on the reattachment length. x_r is seen to decrease from about 0·15 to zero as h increases.‡

† The development length is defined as the smallest value of x beyond which the centre-line velocity differs from its asymptotic value at most by 1 %. P_r is the intercept on the p axis of the asymptote to $p(x)$ curve. Pressure recovery coefficient, as it is conventionally defined, is $2P_r$. In practice, the numerical calculation is terminated when $a_m s$ are sufficiently small to permit the linearization, and (17) is used to extend the computation to downstream infinity (see appendix C).

‡ Reattachment is not obtained with $N \leqslant 5$ for $h = 0{\cdot}9$ and 0·95. More terms are needed for a very small back-step to predict such details accurately.

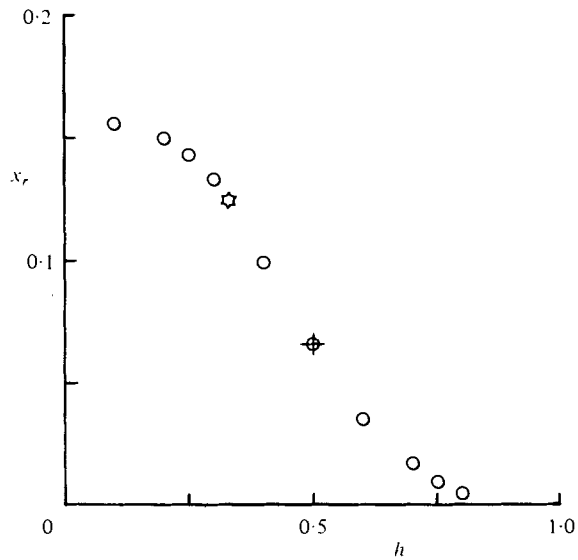

FIGURE 12. The effect of expansion ratio ($1/h$) on the reattachment length. ○, present calculation; ✡, Durst *et al.* (1974), $h = \frac{1}{3}$, $R = 18{\cdot}67$; +, Hung & Macagno (1966), $h = 0{\cdot}5$, $R = 46{\cdot}6$.

Durst, Melling & Whitelaw (1974) have calculated the flow using the Navier–Stokes equation for $h = \frac{1}{3}$. The upstream condition used in their calculation is derived from experiment, and is believed to be parabolic. Their value of x_r is also shown in figure 12, Although R in their calculation is moderately large, x_r obtained by them is in excellent agreement with the present results. Effects of expansion ratio and uniform inlet condition on other quantities is described elsewhere (Kumar & Yajnik 1977).

6.2. *Channel with a base*

The second example considered is the flow behind a base placed symmetrically in a channel (figure 1*b*). The velocity profile upstream of the base is taken to be parabolic,

$$\begin{aligned} u &= 0 \quad 0 \leqslant y \leqslant h, \\ &= 6(y-h)(1-y)/(1-h)^3 \quad h \leqslant y \leqslant 1, \end{aligned} \tag{25}$$

where h is the half-width of the base. The initial condition a_{m0} is then given by

$$a_{m0} = -\frac{12}{G_m(1-h)^2}\left[\theta'_m(h) + \frac{2}{1-h}\theta_m(h)\right]. \tag{26}$$

The initial condition as approximated with different N is shown in figure 13. It is seen that the given initial condition (25) is approximated better as N is increased. Centre-line velocity u_{c0} and the associated momentum flux M_0 given in table 5 show the tendency to approach to their given value with inclusion of higher modes.

The streamline pattern is shown in figure 14. A recirculating region behind the base is obtained, The streamline pattern near the base shows a slight waviness which is probably due to the representation of the initial condition. Table 6 summarizes the main flow features given by the calculation with $N = 5$.

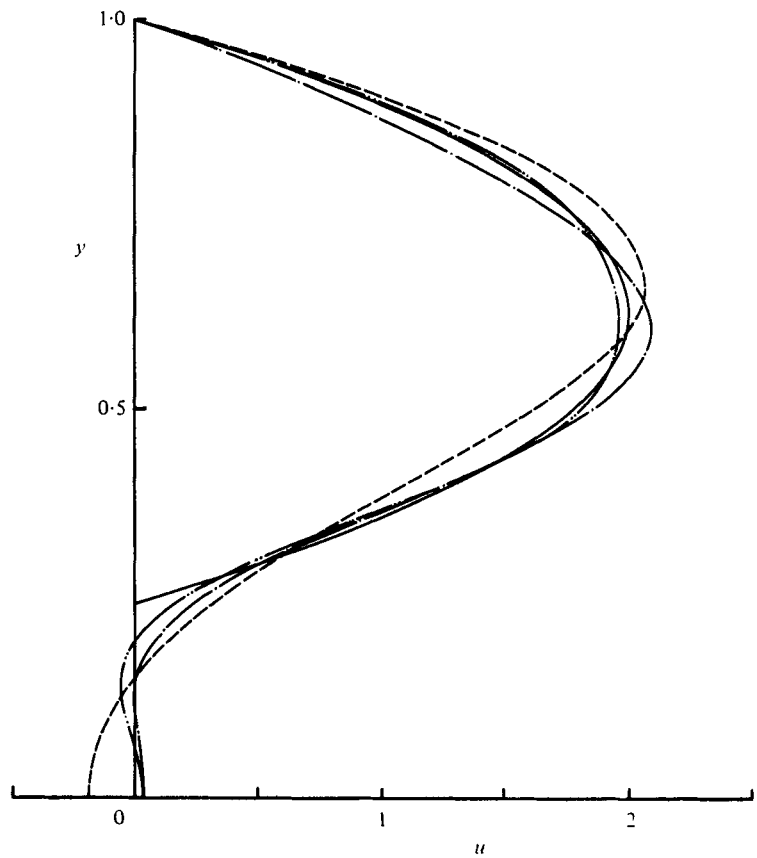

FIGURE 13. Representation of the entry velocity profile for the channel with a base, $h = 0{\cdot}25$. ——, given. Represented: – – –, $N = 2$; —·—·—, $N = 3$; —··—··—, $N = 5$.

N	2	3	5	Given
u_{c0}	−0·1817	0·0368	0·0287	0
M_0	1·6139	1·5978	1·5984	1·6

TABLE 5. Representation of the entry profile for the base in a channel ($h = 0{\cdot}25$).

Mueller & O'Leary (1970) have considered the flow behind a base experimentally as well as numerically. Flow upstream of the base is a uniform flow with a boundary layer. Also a 'lid condition' is imposed on the channel walls which are six base half-widths away from the centre-line. Their calculations show that the ratio of reattachment length to base half-width approaches a value 0·056 times R_h, the Reynolds number used by them. The present calculation gives $x_r/h = 0{\cdot}028$ for parabolic inlet condition. This means that the ratio of reattachment length to base half-width is 0·028 times R. If a Reynolds number based on base half-width and maximum velocity upstream of the base is used, the coefficient of proportionality becomes 0·056. Also, x_c/x_r is 0·343 while that obtained by Mueller & O'Leary is 0·357.

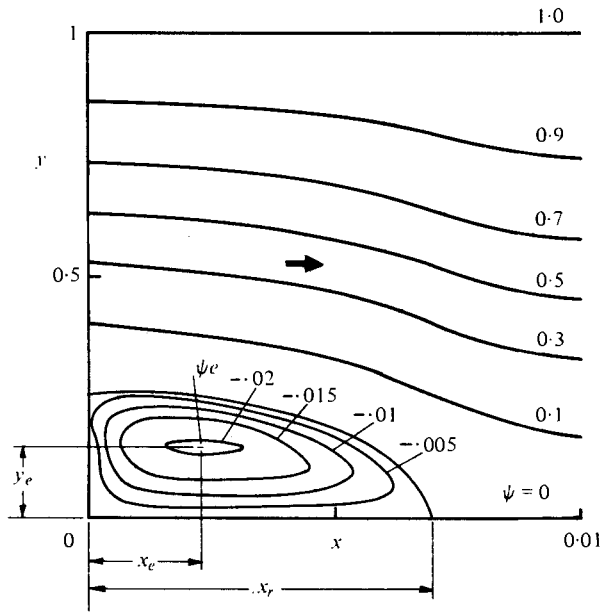

FIGURE 14. Streamlines obtained by the present method for the channel with a base, $h = 0{\cdot}25$, $N = 5$.

Point of reattachment, x_r	0·007
Maximum half-width of the recirculating region	0·264
Location of the centre of the eddy,	
x_e	0·0024
y_e	0·146
Recirculation in one eddy, $-\psi_e$	0·021
Maximum reversed flow velocity at the centre-line	−0·2198
Development length, x_d	0·201
Pressure recovery coefficient, P_r	−0·116

TABLE 6. Base in a channel ($h = 0{\cdot}25$).

7. Concluding remarks

The results obtained by the present method in the first example compare well with those of Hung & Macagno (1966) based on the Navier–Stokes equations, although only a few terms are used in the calculation. Not only the gross quantities of interest such as the length of the recirculating region and the recirculation are found to agree well, but also the streamline pattern. Furthermore, reattachment length calculated by Durst *et al.* (1974) is in good agreement with the present result (figure 12). These comparisons give us confidence in the present method of calculation. In particular, they demonstrate the applicability of the limit equation (4) to this type of internal separated flows.

As the present method requires solution of only a few ordinary differential equations, it is quite simple. A special feature of the method is that the equations (19) have a tendency to get progressively decoupled. It is a consequence of the use of eigenfunctions of the Poiseuille flow development. Further, when the absolute values of

$a_m s$ become sufficiently small, the linearized solution (17) can be employed which adds to the efficiency of the method. Typical computation time is 25 s on IBM 360/44 inclusive of the computation of eigenfunctions.

Appendix A. Axisymmetric internal separated flow

Equations governing the flow are (Macagno & Hung 1967)

$$\frac{1}{r}\psi_x\eta_r - \frac{1}{r}\psi_r\eta_x - \frac{1}{r^2}\eta\psi_x = \frac{1}{R}\left(\eta_{rr} + \frac{1}{r}\eta_r + \eta_{xx} - \frac{1}{r^2}\eta\right), \tag{A 1}$$

$$\eta = \frac{1}{r}\left(\psi_{rr} - \frac{1}{r}\psi_r + \psi_{xx}\right), \tag{A 2}$$

where x and r are the axial and the radial co-ordinates, and ψ the Stokes stream function; R is the Reynolds number.

We have $r \sim 1$ and $\psi \sim 1$. Let the scale of x be L_x. As the flow velocity is bounded $L_x \gtrsim 1$; then $\eta \sim 1$ from (A 2). The left-hand side of (A 1) is of order $1/L_x$ whereas the order of the terms on the right-hand side is $1/R$. The two principal limits are those corresponding to $L_x \sim 1$ and $L_x \sim R$ as obtained for the plane flow. When $L_x \sim 1$, the limit equation is the inviscid equation, while for $L_x \sim R$, viscous terms are of the same order as inertia terms and the limit equation is parabolic. We can once again argue that for the upstream effect $L_x \sim 1$ and the extent of downstream effect is of order R.

It is seen from the calculation of Macagno & Hung (1967) that for large R the length of the separated region downstream of the expansion in a pipe increases linearly with R. A detailed numerical investigation of flow in a pipe with a smooth constriction has been carried out by Deshpande, Giddens & Mabon (1976) who considered four cases of constrictions. For one case the calculations are performed for R up to 2000 and show that the length of the recirculating region forming downstream of the constriction varies linearly with R. Separation upstream of the constriction is not obtained for the range of R considered. However, the region of upstream influence can be assessed from the plots of wall-vorticity and centre-line velocity (see also Deshpande 1977). It is seen that the upstream influence is limited to a short distance and does not show dependence on R, and hence $L_x \sim 1$.

Appendix B. Comments on the equation (19)

Equation (19) is of the form

$$\mathbf{C}\mathbf{a}' = -\mathbf{\Lambda}\mathbf{a}, \tag{B 1}$$

where $\mathbf{a}$ is a N-vector whose elements are $a_1, a_2, \ldots, a_N$, and $\mathbf{C}$ and $\mathbf{\Lambda}$ are $N \times N$ matrices. The derivative $\mathbf{a}'$ can be calculated provided D, the determinant of $\mathbf{C}$, is non-zero. The integration procedure, therefore, can break down for the chosen value of N if D becomes zero at any x. This is a general feature of the integral relations method and is further illustrated by considering the phase space.

The equation governing an integral curve in the N-dimensional phase space whose co-ordinates are $a_1, a_2, \ldots, a_N$, is

$$da_1/D_1 = da_2/D_2 = \ldots = da_N/D_N, \tag{B 2}$$

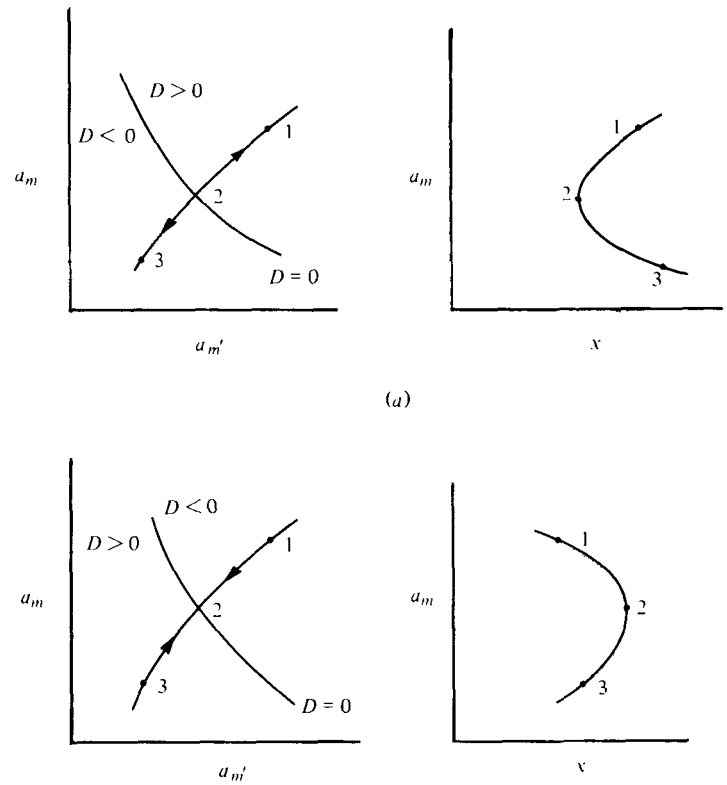

FIGURE 15. Behaviour of an integral curve across $D = 0$. D_m is taken to be positive. The direction in increasing x points outward from $D = 0$ in source type (a) and inward in sink type (b) of singularity.

where D_m is the determinant of the matrix obtained by replacing the mth column of $\mathbf{C}$ by the vector on the right-hand side of (B 1). The evolution of a_m with respect to x, which can be regarded as a parameter of the integral curve $a_m(x)$, can be obtained by solving

$$a'_m = D_m/D. \tag{B 3}$$

The origin of the phase space corresponds to the fully developed flow and therefore a solution describing the flow is expected to approach this point.

D_ms and D are functions of a_ns as (19) is autonomous. They are in fact polynomials of degree N. $D = 0$ would in general represent a surface in the phase space. If an integral curve crosses this surface (figure 15), the direction of increasing x appears either 'sink-like' or 'source-like' and is physically unacceptable for describing the flow. However, an integral curve could cross the surface $D = 0$ at certain critical points† of (B 2). It should be noted that the origin of the phase space is a critical point. If there is a critical point other than the origin then D also vanishes there. This makes it possible for an integral curve to cross at such critical points from one side of the surface $D = 0$ to the other.

† Critical points are points where $D_m = 0$ for $m = 1, 2, \ldots, N$.

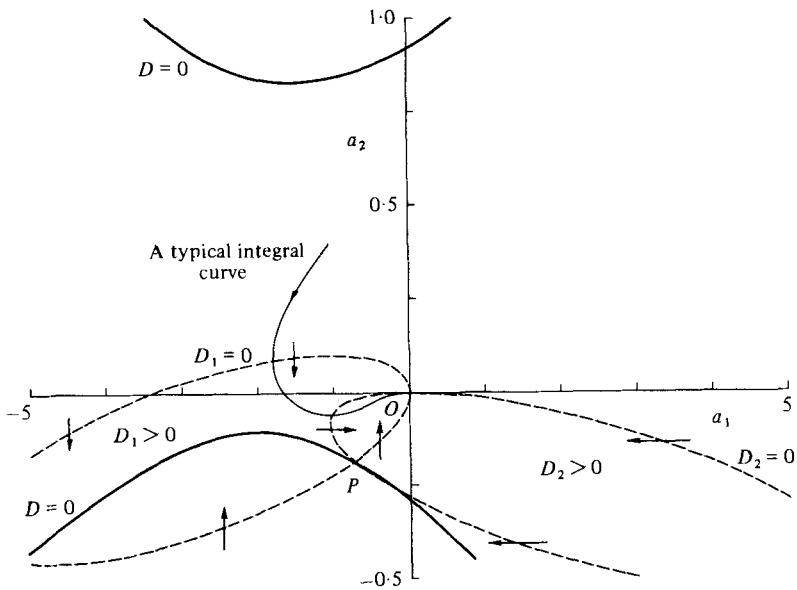

FIGURE 16. Phase plane of symmetric calculation for $N = 2$. The points O and P are critical points. $D_1 = D_2 = 0$ and $D = 1$ at the point O and $D_1 = D_2 = D = 0$ at the point P. Arrows show direction of increasing x.

As an illustration the phase space of symmetric calculation for $N = 2$ is considered in which case D_1, D_2 and D are given by

$$D_1 = -5{\cdot}546a_1^2 + 74{\cdot}79a_1a_2 - 611{\cdot}3a_2^2 - 18{\cdot}81a_1,$$

$$D_2 = -1{\cdot}267a_1^2 - 22{\cdot}23a_1a_2 - 203{\cdot}6a_2^2 - 57{\cdot}55a_2,$$

$$D = 0{\cdot}1796a_1^2 - 0{\cdot}1793a_1a_2 - 3{\cdot}702a_2^2 + 0{\cdot}6947a_1 + 2{\cdot}366a_2 + 1.$$

Figure 16 shows the ellipses $D_1 = 0$ and $D_2 = 0$. The direction of crossing of these ellipses by an integral curve is shown by vertical and horizontal arrows. A typical integral curve is also shown in the figure.

The origin, which is a critical point, is a stable two-tangent node with a_1 axis as the tangent. Figure 16 shows another critical point P which is found to be a saddle point. The neighbourhood of the critical point P is considered below.

Figure 17 shows a schematic of a saddle point singularity. Open arrows show the direction of x increasing if D were positive everywhere. Now let us draw the curve $D = 0$ passing through the saddle point. The direction of x increasing is then shown by filled arrows which shows that an integral curve can cross the curve $D = 0$ at the critical point P that is physically acceptable. The source- or sink-like behaviour of the integral curves are seen at points other than P of the curve $D = 0$.

The occurrence of $D = 0$ on an integral curve in general renders the calculation physically inadmissible. However, under some specific condition $D = 0$ can be admitted on an integral curve. Such integral curves are unlikely to represent a physical situation as their neighbouring integral curves would in general be physically inadmissible. Also, such curves are special to the phase space of N-term calculation.

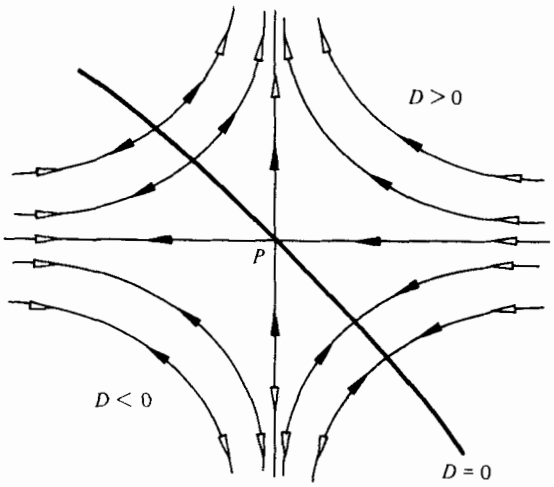

FIGURE 17. Schematic of a saddle point singularity on $D = 0$. Filled arrows show direction of increasing x. Open arrows show direction of increasing x if D were greater than zero at all points.

If for a given initial condition the integral curve of N-term calculation encounters $D = 0$, it can be hoped that this difficulty can be overcome by including more terms in the calculation.

Appendix C. Development length and pressure recovery coefficient

Development length

The development length x_d satisfies

$$|u_c(x) - 1{\cdot}5|/1{\cdot}5 \leqslant 0{\cdot}01 \quad \text{for} \quad x \geqslant x_d. \tag{C 1}$$

If x_0 is a streamwise location after which the linearized solution (17) is applicable, then x_d can be obtained from

$$\left| \sum_m a_m(x_0) \exp\{-\lambda_m(x_d - x_0)\}.\phi'_m(0) \right| = 0{\cdot}015.$$

The contribution of the modes higher than the first even mode can be neglected as they decay more rapidly. x_d can then be obtained from

$$x_d = x_0 - (1/\lambda_{e1}) \ln |0{\cdot}015/a_{e1}(x_0)|, \tag{C 2}$$

where the subscript $e1$ denotes the first even mode.

Pressure recovery coefficient

The asymptote to the curve $p(x)$ is given by

$$p = -3x + P_r. \tag{C 3}$$

If the linearized solution (17) is applicable for $x \geqslant x_0$, P_r can be calculated from

$$P_r = p(x_0) + 3x_0 + \sum_m a_m(x_0)\phi'''_m(1)/\lambda_m. \tag{C 4}$$

REFERENCES

BATCHELOR, G. K. 1956 On steady laminar flow with closed streamlines at large Reynolds number. *J. Fluid Mech.* **1**, 177–190.

CARTER, J. E. 1975 Inverse solution for laminar boundary layer flows with separation and reattachment. *N.A.S.A. Tech. Rep.* R-447.

CATHERALL, D. & MANGLER, K. W. 1966 The integration of the two-dimensional laminar boundary-layer equations past the point of vanishing skin friction. *J. Fluid Mech.* **26**, 163–182.

CHENG, R. T. 1972 Numerical solution of the Navier–Stokes equations by the finite element method. *Phys. Fluids* **15**, 2098–2105.

DESHPANDE, M. D. 1977 Steady laminar and turbulent flow through vascular stenoses model. Ph.D. thesis, Georgia Inst. of Tech., Atlanta.

DESHPANDE, M. D., GIDDENS, D. P. & MABON, R. F. 1976 Steady laminar flow through modelled vascular stenoses. *J. Biomech.* **9**, 165–174.

DORODNITSYN, A. A. & MELLER, N. A. 1970 Application of the small parameter method to the solution of Navier–Stokes equations. *Fluid Dyn. Trans.* **5** (II), 67–82.

DURST, F., MELLING, A. & WHITELAW, J. H. 1974 Low Reynolds number flow over a plane symmetric sudden expansion. *J. Fluid Mech.* **64**, 111–128.

FRIEDMAN, M. 1972 Laminar flow in a channel with a step. *J. Engng Math.* **6**, 285–290.

GILLIS, J. & BRANDT, A. 1964 The numerical integration of the equations of motion of a viscous fluid. *Weizmann Institute Rep.* AF EOAR 63-73 SR-1.

GREENSPAN, D. 1969 Numerical studies of steady viscous, incompressible flow in a channel with a step. *J. Engng Math.* **3**, 21–28.

HUNG, T. K. & MACAGNO, E. O. 1966 Laminar eddies in a two-dimensional conduit expansion. *La Houille Blanche* **21**, 391–401.

KITCHENS, C. W. 1974 Calculation of low Reynolds number flow past a square protuberance. *A.I.A.A. J.* **12**, 1005–1007.

KLEMP, J. B. & ACRIVOS, A. 1972 A method for integrating the boundary-layer equations through a region of reverse flow. *J. Fluid Mech.* **53**, 177–191.

KLINEBERG, J. M. & STEGER, J. L. 1974 The numerical calculation of laminar boundary-layer separation. *N.A.S.A. Tech. Note* D-7732.

KOVASZNAY, L. I. G. 1948 Laminar flow behind a two-dimensional grid. *Proc. Camb. Phil. Soc.* **44**, 58–62.

KUMAR, A. 1976 Analysis and calculation of internal separated flow at large Reynolds number. Ph.D. thesis, IIT Kanpur.

KUMAR, A. 1977 Eigenfunctions of the Poiseuille flow development. *NAL Bangalore Rep.* AE-TM-15-77.

KUMAR, A. 1978 On the solution of the boundary layer equation in the presence of reverse flow. *NAL Bangalore Rep.* AE-TM-9-78.

KUMAR, A. & YAJNIK, K. S. 1976 Poiseuille flow development by eigenfunction expansion method. *NAL Bangalore Rep.* AE-TM-19-76.

KUMAR, A. & YAJNIK, K. S. 1977 Flow in a channel with a symmetric sudden expansion. *6th Australasian Hydraulics and Fluid Mech. Conf., Adelaide.*

MACAGNO, E. O. & HUNG, T. K. 1967 Computational and experimental study of a captive annular eddy. *J. Fluid Mech.* **28**, 43–64.

MORIHARA, H. 1972 Numerical integration of the Navier–Stokes equations. Ph.D. thesis, State U. of New York at Buffalo.

MUELLER, T. J. & O'LEARY, R. A. 1970 Physical and numerical experiments in laminar incompressible separating and reattaching flows. *A.I.A.A. Paper* no. 70–763.

NALLASAMY, M. 1975 Numerical studies on laminar internal separated flow. Ph.D. thesis, IISc Bangalore.

PRANDTL, L. 1904 Motion of fluid with very little viscosity. English Translation: *N.A.S.A.* TM 452, 1928.

ROACHE, P. J. & MUELLER, T. J. 1970 Numerical solutions of laminar separated flows. *A.I.A.A. J.* **8**, 530–538.

SCHLICHTING, H. 1934 Laminare Kanaleinlaufströmung. *Z. angew. Math. Mech.* **14**, 368–373.

SMITH, F. T. 1977 Upstream interactions in channel flows. *J. Fluid Mech.* **79**, 631–656.

TAYLOR, T. D. & NDEFO, E. 1970 Computation of viscous flow in a channel by the method of splitting. *II Intl. Conf. on Numerical Methods in Fluid Dyn.*, pp. 356–364.

WANG, Y. L. & LONGWELL, P. A. 1964 Laminar flow in the inlet section of parallel plates. *A.I.Ch.E. J.* **10**, 323–329.

WILSON, S. 1969 The development of Poiseuille flow. *J. Fluid Mech.* **38**, 793–806.